ELSEVIER

Journal of Power Sources 97–98 (2001) 39–46

JOURNAL OF POWER SOURCES

www.elsevier.com/locate/jpowsour

# The complex electrochemistry of graphite electrodes in lithium-ion batteries

Petr Novák*, Felix Joho, Martin Lanz, Beat Rykart, Jan-Christoph Panitz[1], Dario Alliata[2], Rüdiger Kötz, Otto Haas

*Laboratory for Electrochemistry, Paul Scherrer Institute, CH-5232 Villigen PSI, Switzerland*

Received 20 June 2000; accepted 30 December 2000

**Abstract**

This paper discusses the interrelated phenomena of solid electrolyte interphase (SEI) formation and the irreversible charge consumption which occurs during the first cycle of a graphite electrode, as well as their relevance to the cycling stability of lithium-ion batteries. Thus, results from relevant characterization methods, namely, in situ mass spectrometry, in situ infrared spectroscopy, in situ Raman and video microscopy, in situ scanning probe microscopy, in situ quartz crystal microbalance, and differential scanning calorimetry were combined for a more thorough understanding of observations made in cycling experiments. From electrochemical cycling tests, we have learned that a high specific charge (~360 Ah/kg of carbon), satisfactory cycle life of the graphite electrodes (1000 deep cycles), and an irreversible charge of <7% during SEI formation can only be obtained when water contamination of the cell is avoided. Under such conditions, a good-quality SEI film is formed on the carbon surface. We conclude that during SEI film formation, at first the carbonate solvent(s) are reduced, forming ethylene gas, organic radicals, oligomers, and polymers. Then a SEI film is precipitated on the surface via a nucleation and growth mechanism. The irreversible charge consumption due to SEI formation is proportional to the BET specific surface area of the graphite and rapidly increases with increasing water content in the cell. 

*Keywords:* Lithium-ion cell; Graphite electrode; SEI film; Electrolyte decomposition; In situ methods

## 1. Introduction

Commercial lithium-ion cells with high energy density and good cyclability consist of a carbon-based negative electrode, a positive lithium metal oxide electrode, and a separator soaked with an organic electrolyte [1]. Most commercial cells manufactured today use graphitic carbons [2]. Much knowledge has been gained about graphites in recent years [3–5], but some important scientific challenges still remain. One of them is the comprehensive understanding of the surface phenomena associated with the irreversible charge consumption occurring during the first cycles of the graphite electrodes [6]. It is generally accepted that this charge consumption is mainly due to reductive decomposition of the electrolyte on the negative electrode [7]. The resulting protective film, called solid electrolyte interphase (SEI), allows lithium-ion transfer but prevents electron transfer [8]. The SEI formation mechanism is rather complex and still subject of controversial scientific discussions [9].

It is the aim of this paper to discuss the interrelated phenomena of SEI formation and the irreversible charge consumption which occur during the first cycle of a graphite electrode [10], as well as their relevance to the cycling stability of graphite electrodes in lithium-ion batteries [11]. Thus, results from relevant advanced characterization methods, namely, in situ mass spectrometry, in situ infrared spectroscopy, in situ Raman and video microscopy, in situ scanning probe microscopy, in situ quartz crystal microbalance, and differential scanning calorimetry were combined for a more thorough understanding of observations made in cycling experiments.

## 2. Experimental

The experiments were performed at room temperature using a 1 M solution of $LiPF_6$ (Merck) or $LiClO_4$ (Merck) in

* Corresponding author. Tel.: +41-56-310-2457; fax: +41-56-310-4415.
*E-mail address*: petr.novak@psi.ch (P. Novák).
[1] Present address: Chemetall GmbH, Trakehner Strasse 3, DE-60487 Frankfurt am Main, Germany.
[2] Present address: I.N.F.M.-Dipartimento di Scienze Ambientali, Università della Tuscia, IT-01100 Viterbo, Italy.

0378-7753/01/$ – see front matter 
PII: S0378-7753(01)00586-9

a 1:1 mixture of ethylene carbonate (EC, Merck) and dimethyl carbonate (DMC, Merck). The water content of the electrolytes as determined by Karl–Fischer titration was <10 ppm unless otherwise indicated. The HF content in $LiPF_6$-based electrolytes was about 50 ppm. Either lithium metal or $LiMn_2O_4$ (BASF) were used as the counterelectrode. Metallic lithium was the reference electrode. All potentials throughout the paper are reported with reference to the $Li/Li^+$ couple.

*Galvanostatic cycling experiments* were performed either in coin cells or in laboratory test cells [12]. The working electrodes were in most cases prepared from TIMREX® synthetic graphites (TIMCAL Group, Bodio, Switzerland). The values of the Brunauer–Emmett–Teller (BET) specific surface area of the graphite samples were provided by the manufacturer. Details of electrode preparation and cycling procedures are described elsewhere [11,13]. For the determination of the irreversible charge consumption, we chose slow cycling conditions of ca. C/40. Therefore, most of the irreversible charge consumption occurred during the first cycle, which was performed galvanostatically between 1.5 and 0.005 V at a rate of ±0.01 mA/mg (related to the graphite mass). At 0.005 V, the current was lowered potentiostatically to 0.005 mA/mg. The irreversible charge consumption is defined as the difference between the cathodic and anodic charge of the first cycle, given in percent relative to the total cathodic charge ($Li^+$ insertion).

Both in situ *Raman spectroscopy* and in situ *video microscopy* experiments were performed with a confocal Raman microscope (LabRam, DILOR/Instruments SA) using the 530.901 nm line of an external $Kr^+$ ion laser in a spectroelectrochemical cell of special design [14]. The lateral resolution of the Raman map recorded from the surface of the working electrode (located below a glass optical window) was ca. 4 μm according to the manufacturer's specification when using a microscope objective with an ultralong working distance and a magnification of 50×. The microscope was equipped with a video camera as well, so that the charging and discharging of the cell could be followed using video microscopy, with a magnification of about 400×. As shown below, Raman spectra could be recorded with an *S:N* ratio that has been improved by a factor of about 100, as compared to our previous work [15].

In situ *atomic force microscopy* (AFM) experiments were performed inside a glove box filled with argon using an Autoprobe CP (Park Scientific Instruments) equipment. The experimental details were published elsewhere [16]. The working electrode was a highly oriented pyrolytic graphite (HOPG) ZYH-type crystal (Advanced Ceramics Corporation, Lakewood, OH). The water content of the electrolyte was <50 ppm in this case.

*Electrochemical quartz crystal microbalance* (EQCM) experiments were performed with 5 MHz, AT-cut quartz crystals (Vectron International, Neckarbischofsheim, Germany) having a diameter of 15 mm, with 0.3 $cm^2$ active surface area of titanium sputter-deposited in a keyhole shape (thickness ca. 1000 Å). The active area of the crystal was coated with graphite by spraying a slurry of 95 wt.% of graphite TIMREX® SFG 6 and 5 wt.% of PVDF/HFP copolymeric binder (Solef 20810, Solvay) onto the crystal with an air-brush. The loading of the electrode was less than one layer of graphite particles (the average particle size of graphite SFG 6 is about 3 μm). The quartz crystal was fixed with silicone adhesive at the bottom of a polypropylene cell body. The graphite electrode was cycled with a scan rate of 1 mV/s between 2.0 and 0.0 V, but starting the first reductive sweep at 3.0 V (close to the initial open-circuit electrode potential). Potential, current, and frequency of the oscillating crystal were recorded simultaneously during cycling.

*Differential electrochemical mass spectrometry* (DEMS) was used for the identification of gaseous and volatile products evolved at the graphite electrode during cycling. The apparatus, the DEMS cell, and the procedure for preparing working electrodes are described in [17–19]. The graphite loading varied between ca. 0.5 and 15 mg/$cm^2$. The latter value corresponds to that typically used in commercial lithium-ion cells [20]. The DEMS measurements were carried out potentiodynamically with a scan rate of 0.4 mV/s. The current (CV) and the mass signals (MSCV) were recorded simultaneously as functions of potential.

Carbon electrodes for *differential scanning calorimetry* (DSC) were prepared from a slurry containing various carbons and 10% PVDF in 1-methyl-2-pyrrolidone, which was coated by the doctor-blade technique on a copper foil. The electrodes were cut into disks 13 mm in diameter. These electrodes were cycled against lithium metal, which was both counter and reference electrode. After one cycle or 1.5 cycles, the copper current collector was removed in the glove box, and the electrode mass was cut into 4 mm-diameter disks and immediately placed into stainless steel sample capsules without washing. DSC measurements were carried out on a Perkin-Elmer DSC7 apparatus with a heating rate of 10 K/min from 30 to 300°C.

## 3. Results and discussion

During the last decade, a vast amount of highly contrary experimental results have been published on the electrochemical behavior of graphite electrodes in lithium-ion cells. The differences in the published numbers are immense, even for identical materials in the same electrolyte solution. It is our experience that both the preparation technique and the drying procedure of graphite working electrodes are crucial for their electrochemical performance. From electrochemical cycling tests of carefully prepared electrodes based on TIMREX® graphites (using both spray and doctor-blade techniques), we have learned that a high specific charge (∼360 Ah/kg of carbon) can be obtained independently of the graphite type. The cycle life of graphite electrodes is satisfactory, both when using lithium metal [11] and when using an oxide as the counterelectrode (Fig. 1).

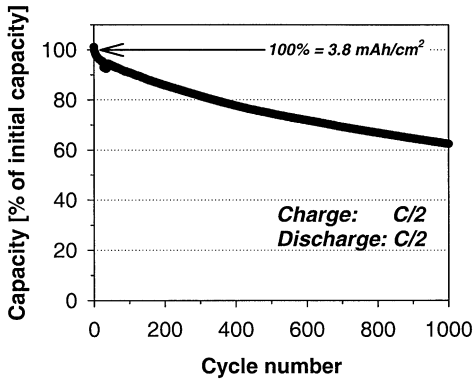


Fig. 1. Cycle performance at C/2 of a coin cell containing graphite TIMREX® SLM 44 and $LiMn_2O_4$ spinel (BASF) as electrode materials, and 1 M $LiPF_6$ + EC/DMC as the electrolyte. In each given cycle, the cell was cycled to 100% of the capacity exhibited in the last prior cycle (initially 3.8 mAh/cm$^2$).

The charge consumed due to side reactions in the first cycle (''irreversible charge'', in technical literature frequently called the ''charge loss'') is <7% at low scan rates for graphites with low BET specific surface areas (Fig. 2). However, this low value as well as the good cycleability can only be obtained when water contamination of the cell is avoided. As reported earlier by us, the irreversible charge consumption rapidly increases with increasing water content in the cell, e.g. from about 20% (<10 ppm $H_2O$) to about 40% (~1500 ppm $H_2O$) for the high-surface-area graphite SFG 6 in a $LiClO_4$-based electrolyte [11]. Moreover, the scatter of the results rapidly increases with increasing water content.

The irreversible reactions consume lithium. This decreases the charge and energy density of the cell. Therefore, the irreversible charge consumption should be minimized. In our simple model [21,22], we distinguish between three types of irreversible charge consumption (Fig. 2): (i) the irreversible charge related to the reduction of the surface groups of graphite between ca. 3 and 0.8 V versus Li/Li$^+$, (ii) the irreversible charge due to SEI formation via electrolyte decomposition between ca. 0.8 and 0.2 V, and (iii) the

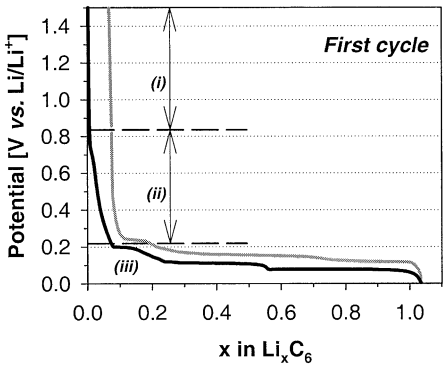


Fig. 2. First galvanostatic charge/discharge cycle at ~C/40 of a graphite TIMREX® E-SLX 50 electrode in the 1 M $LiPF_6$ + EC/DMC electrolyte.

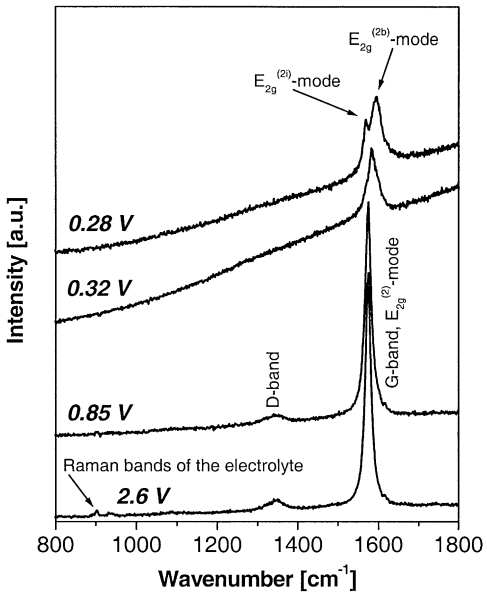


Fig. 3. In situ Raman spectra measured at indicated potentials at a single carbon particle at the surface of a commercial negative electrode during the first charging at 0.1 mA/cm$^2$ (~C/30) in the 1 M $LiClO_4$ + EC/DMC electrolyte. The spectra were arbitrary shifted on the vertical scale.

irreversible charge due to side reactions parallel to the reversible intercalation and de-intercalation of lithium ions (corrosion-like reactions of $Li_xC_6$ which contribute to the SEI film growth). It can be clearly seen from Fig. 2 that the main contribution to the irreversible charge consumption is in the region (ii) where the SEI is essentially formed.

For a deeper insight into the processes at the graphite/electrolyte interface, several surface-sensitive in situ methods were employed. First, we applied in situ Raman microscopy. The typical spectra shown in Fig. 3 were recorded on a single carbon particle arbitrarily selected on the surface of a commercial negative electrode (Fig. 4). It should be noted that in contrast to previous work, the bands from bulk electrolyte contribute little to the total intensity recorded, since the cell design has been improved and only the amount of electrolyte necessary for optimum electrochemical performance of the cell was added. With decreasing electrode potential, changes in the Raman spectra were observed that agree with results obtained earlier [15,23]. The $E_{2g}^{(2)}$-mode of graphite splits into two modes that can be assigned to $E_{2g}^{(2)}$ vibrational modes of graphene sheets adjacent to a lithium layer ($E_{2g}^{(2b)}$, displaced to higher wavenumber) and to $E_{2g}^{(2)}$ vibrational modes of graphene sheets adjacent to other graphene sheets ($E_{2g}^{(2i)}$). In addition, upon formation of the lithium-intercalated graphite compound, the D-band is no longer observed (Fig. 3).

Using in situ video microscopy, further information can be obtained. Fig. 4 shows video micrographs recorded at the same spot that had been examined with Raman microscopy. The top picture shows the electrode shortly after cell assembly, at open circuit. Particles made of graphitic carbon can be discerned against the darker mesocarbon microbeads

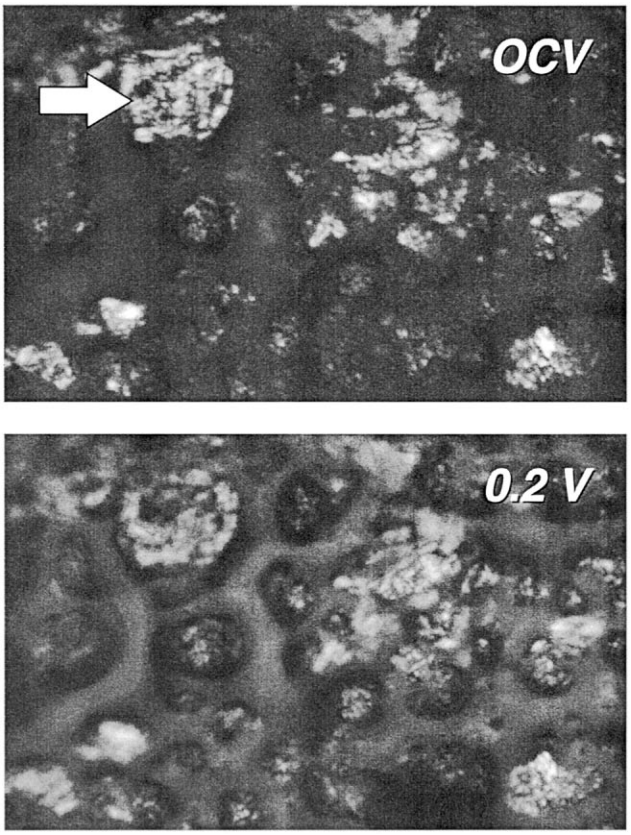


Fig. 4. In situ video micrographs recorded at the surface of a commercial negative electrode at open circuit (shortly after cell assembly, top) and at ca. 0.2 V vs. Li/$Li^+$ (after first reduction with 0.1 mA/$cm^2$, bottom) in the 1 M $LiClO_4$ + EC/DMC electrolyte. The arrow indicates the carbon particle where the Raman spectra shown in Fig. 3 were recorded.

(MCMB) particles. The bottom picture illustrates the changes that have taken place during the first reduction of the electrode. This image was recorded at ca. 0.2 V versus Li/$Li^+$. Compared to the image on top, it appears that the electrolyte has receded into channels which appear to be filled with an opaque viscous liquid. This result might indicate that the SEI layer is thicker in the channels between the particles, but further experiments must be performed to confirm this hypothesis.

In dry EC-based electrolytes, a significant reduction current is observed at potentials $\leq$0.8 V versus Li/$Li^+$ (Fig. 2). At ~0.8 V, ethylene gas starts to evolve which can be detected by in situ mass spectrometry (DEMS). In cyclic voltammetric experiments on graphite electrodes, the mass signals of ethylene fragments correlate well with a negative current peak corresponding to SEI formation [17]. Thus, it is clear from both galvanostatic and CV experiments that the appearance of ethylene gas mass signals documents SEI formation reactions. Consequently, the main SEI formation reaction(s) start(s) at ca. 0.8 V versus Li/$Li^+$ in EC-based electrolytes. Besides, hydrogen gas can also be detected by the DEMS method when water is present in the electrolyte solution, in which case the amount of ethylene evolved appears to be lower. No other volatile products were detected.

From in situ measurements, we know that the infrared spectra and, thus, the SEI layers are similar on different carbons [10]. For convenience, therefore, we chose the basal surface of HOPG for our SEI morphology studies. We have noticed that during potential sweeps in EC/DMC-based electrolytes, the morphology changes due to SEI formation can be detected at ca. 0.7 V (Fig. 5), which is shortly after the start of ethylene evolution. The in situ AFM technique revealed that the SEI is very rough at first (Fig. 6), and does not cover the whole surface of the electrode, but later on the SEI film is about 200 Å thick and covers the entire surface. From the literature, it is known that the SEI film contains alkyl carbonates, $Li_2CO_3$, and salt reduction products [24]. Actually, it has been confirmed by in situ TEM studies that the SEI film is of dual nature, organic and inorganic [25]. A plausible model suggests that the SEI layer contains polymer-like substances with repeating oxyethylene units similar to polyethylene oxide [26]. Moreover, it has been suggested that the SEI is formed mainly by decomposition of EC [26].

Our in situ EQCM experiments give some deeper insight into this process. As can be seen from Fig. 7, the mass of the graphite electrode increases as expected during lithium intercalation and decreases during the reverse process. A distinct frequency decrease (mass increase) peak centered around 0.7 V which is related to SEI precipitation can be recognized in the frequency response of the quartz crystal. Taking a closer look, this frequency decrease even starts before a distinct electrochemical SEI precipitation current starts to flow. A decreased frequency of the EQCM can be explained by either higher electrode mass or by increased viscosity of the environment. The observed negative frequency shift may be caused by increased viscosity of the electrolyte solution in the vicinity of the electrode. Due to the electrochemical charging of the electrode surface, lithium ions coordinated with EC, which is the high-viscosity component of the electrolyte solution, are attracted by the electrode, thereby increasing the electrolyte viscosity in the vicinity of the electrode. The small positive frequency shift starting at ca. 0.7 V can be explained by the consumption of EC due to SEI formation and ethylene formation, because both processes decrease the electrolyte viscosity in the vicinity of the electrode.

Thus, combining our results with literature data, we can conclude at this point that at first the ethylene carbonate solvent is reduced, forming ethylene gas, organic radicals, oligomers, and polymers. Then a SEI film is precipitated on the surface of the carbon via a nucleation and growth mechanism. All these observations conform that the formation of the SEI is a complex process which among other things depends on the amount of trace water present in the cell. Besides, the DEMS experiments show that ethylene gas evolution is complete within very short periods of time on thin (<10 μm) model electrodes, but on electrodes about

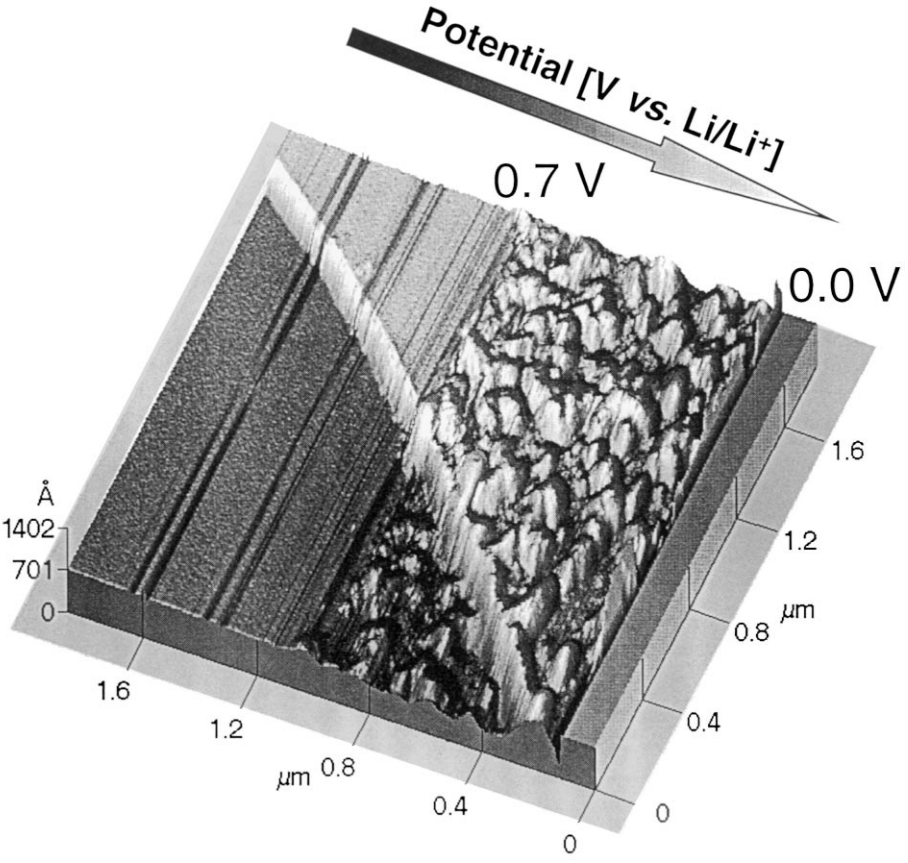


Fig. 5. In situ AFM image showing the SEI formation in 1 M $LiClO_4$ + EC/DMC electrolyte on a step at the basal surface of a HOPG electrode. The image was recorded at one line per second during a 5 mV/s potential sweep from 1.3 to 0 V vs. $Li/Li^+$.

100 μm thick as in the example of Fig. 8, much more time is required for formation of an effective SEI film, and ethylene gas continues to be generated even at open circuit when the potential of the (lithiated) graphite electrode is more negative than ∼0.8 V.

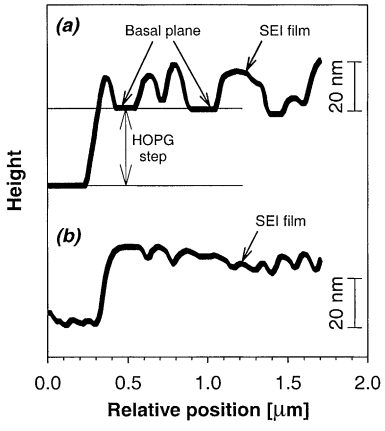


Fig. 6. Vertical surface profile from in situ AFM images showing the same step as in Fig. 5 at the basal surface of a HOPG electrode in 1 M $LiClO_4$ + EC/DMC. Trace (a) corresponds to a potential of 0.25 V vs. $Li/Li^+$ in Fig. 5 and shows SEI islands about 15 nm in height. Trace (b) shows the surface profile recorded when SEI growth was complete (the corresponding AFM image was acquired at 3 V after 2 cycles at 5 mV/s).

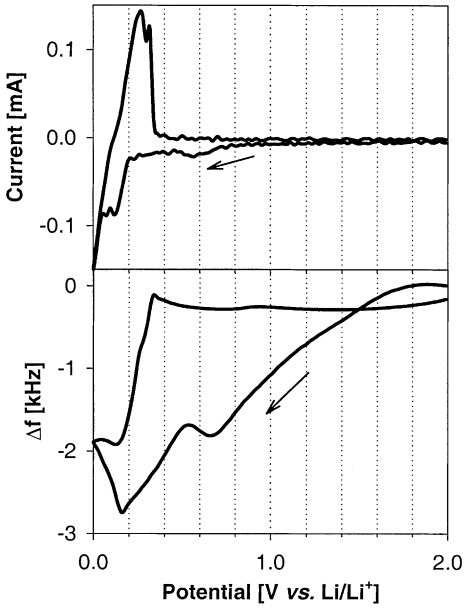


Fig. 7. Cyclic voltammogram at 1 mV/s and a typical EQCM response of a graphite TIMREX® SFG 6 electrode in 1 M $LiPF_6$ + EC/DMC electrolyte.

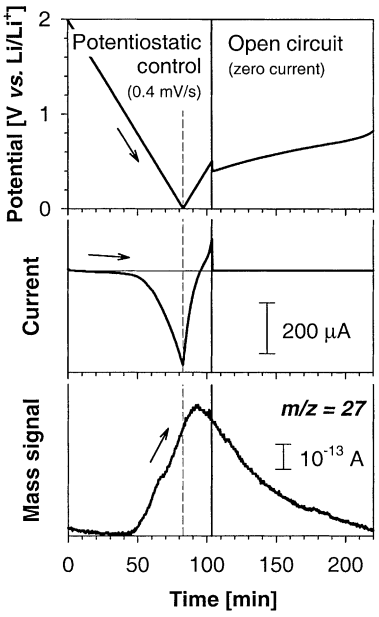


Fig. 8. DEMS experiment with an ~100 μm graphite sheet electrode in 1 M $LiPF_6$ + EC/DMC (second cycle at 0.4 mV/s followed by an open-circuit step). The mass signal $m/z = 27$ represents ethylene.

Finally, it should be noted that SEI formation is a strictly surface-related process. Provided that the electrodes are fully wetted with the electrolyte, there should be a linear dependence of the irreversible charge consumption on the BET specific surface area of the graphites. A similar dependence [13] exists between the irreversible charge consumption and the double-layer capacity of graphite electrodes. We show elsewhere [13] that both synthetic and natural graphites nicely adhere to this linearity. Thus, from the BET specific surface area of a particular graphite type, the irreversible charge consumption in a lithium-ion cell can be directly estimated using the correlation shown in Fig. 9. Actually, there is a small irreversible charge of about 2.5% when extrapolating the correlation to zero BET area. This is an indication that minor volume-based reactions must be also considered. The latter are probably associated with reduction of the binder, reduction of impurities in the electrolyte solution, and/or reduction of some oxygen-containing groups located on defect sites within the graphite structure.

An important question remaining open at this point concerns the safety of graphite electrodes during their entire cycle life. According to the literature [27], the positive electrode, containing usually the highly oxidized compound $LiCoO_2$, above 220°C may evolve atomic oxygen, which will react with the organic solvent of the electrolyte solution. As a result, a large amount of energy is released. The SEI layer formed on carbon electrodes gives off heat at temperatures around 100°C, the onset temperature for the breakdown of the SEI layer being strongly dependent on the lithium salt used in the electrolyte [28]. The thermal effect is much smaller than that observed with the positive electrodes, but the question should be raised whether the heat evolved might bring the cell to temperatures of up to 220°C where oxygen evolution occurs, which then may cause a thermal runaway of the cell.

DSC was used for studies of the heat evolution of graphite electrodes. Generally, cycled carbon electrodes evolve heat within two temperature ranges (Fig. 10). In $LiPF_6$-containing electrolytes, a small heat evolution occurs at 120–150°C, which is attributed to the decomposition of the SEI layer on carbon [29]. A larger heat evolution occurs at 270–300°C, and is attributed to decomposition of the electrode binder. The heat evolution from fully charged electrodes is more pronounced than that from cycled but discharged electrodes (Fig. 10). Thus, the negative graphite electrodes are potentially more dangerous when they are fully charged. The same had been found for positive electrodes [1].

In view of their highly different surface areas, cell safety should also depend on the type of graphites used. We compared the heat evolution of four different types of graphite. In Fig. 11, we show the estimated temperature increase in a hypothetical cylindrical cell of the 18650 type (known as the original SONY cell). We assumed that the cell

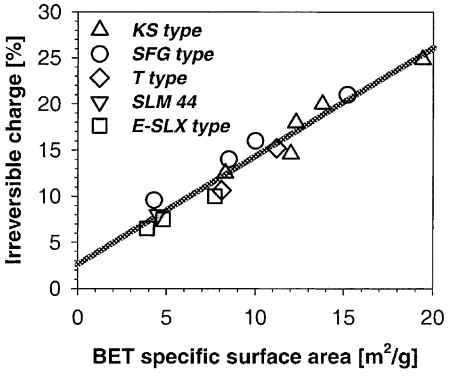


Fig. 9. Irreversible charge consumption in the first cycle at ~C/40 (as in Fig. 2) of TIMREX® graphites in the 1 M $LiPF_6$ + EC/DMC electrolyte as a function of the graphite BET specific surface area.

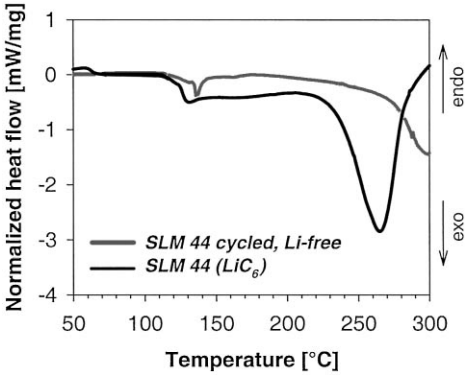


Fig. 10. Typical DSC traces at 10 K/min of lithium-free graphite (after 1 electrochemical cycle) and $LiC_6$ (after 1.5 cycles); the electrolyte was 1 M $LiPF_6$ + EC/DMC.

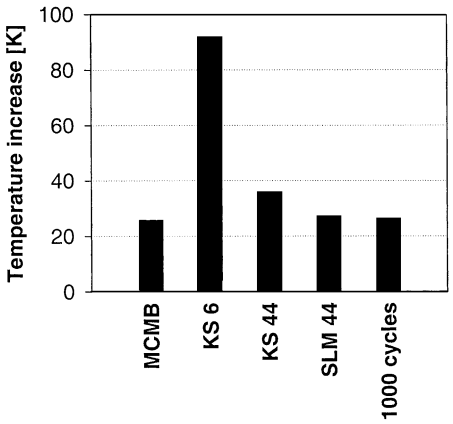


Fig. 11. Temperature increase in a cylindrical 1.4 Ah SONY 18650 cell, estimated from DSC measurements while assuming different carbons to be present in the negative electrode (1000 cycles denotes a DSC measurement on a TIMREX® SLM 44 electrode after the cycling experiment shown in Fig. 1).

has a capacity of 1.4 Ah, a weight of 39.4 g, and a specific heat of 0.92 J/(g K) [30]. The estimated cell temperature increase is almost 100 K when it is assumed that a graphite with a high specific surface area (KS 6, 19.4 $m^2$/g) would be used. The estimated temperature increase for the other two types of synthetic graphite (KS 44, 8.3 $m^2$/g and SLM 44, 4.5 $m^2$/g) and for MCMB 10–28 (a highly graphitized carbon containing less crystalline regions often used in commercial electrodes, having 2.5 $m^2$/g [31]) would be only about 30 K.

The properties of the electrochemical systems change during use. Therefore, we also investigated the electrode of a cell which was fully charged and discharged 1000 times (cf. Fig. 1). The cycling experiment lasted about 6 months. The cycled graphite SLM 44 electrode showed a completely different DSC trace than found for the original material, which indicates that the SEI layer was transformed during cycling. However, the amount of heat evolved did not change significantly, and is such that it would be able to raise the temperature of the cell by only about 30 K.

## 4. Conclusions

It follows from the experiments that graphites with low BET specific surface area (<10 $m^2$/g) are safe electroactive materials suitable for negative electrodes of lithium-ion cells. The cycling stability of graphite electrodes is high provided that an effective SEI layer is formed on their surface. The irreversible charge consumption due to SEI formation in the first cycle is proportional to the BET specific surface area of the graphite. It is important to keep in mind that the SEI formation is a complex process which can be influenced by many factors. Among other things, the amount of trace water present in the cell must be low to form an effective SEI and to achieve satisfactory performance of the graphite electrode.

Raman microscopy is a valuable tool to investigate the degree of intercalation on the surface of a graphite electrode in situ. The formation of the SEI layer can be directly observed with in situ AFM. DSC and DEMS are helpful methods to investigate safety aspects of graphite electrodes like the development of gases at the electrode and heat evolution due to SEI decomposition.

## Acknowledgements

This work was supported in part by the Swiss Federal Office of Energy, Swiss National Science Foundation, and TIMCAL Group. We are grateful to Dr. M.E. Spahr, TIMCAL Group, for graphite samples and numerous stimulating discussions.

## References

[1] M. Broussely, P. Biensan, B. Simon, Electrochim. Acta 45 (1999) 3.
[2] T. Zheng, J.R. Dahn, Applications of carbon in lithium-ion batteries, in: T.D. Burchell (Ed.), Carbon Material of Advanced Technology, Pergamon Press, Oxford, UK, 1999, p. 341.
[3] D. Aurbach, B. Markovsky, I. Weissman, E. Levi, Y. Ein-Eli, Electrochim. Acta 45 (1999) 67.
[4] A. Funabiki, M. Inaba, T. Abe, Z. Ogumi, Electrochim. Acta 45 (1999) 865.
[5] A.M. Andersson, K. Edström, J.O. Thomas, J. Power Sources 81/82 (1999) 8.
[6] Y. Ein-Eli, Electrochem. Solid State Lett. 2 (1999) 212.
[7] D. Aurbach, B. Markovsky, M.D. Levi, E. Levi, A. Schechter, M. Moshkovich, Y. Cohen, J. Power Sources 81/82 (1999) 95.
[8] E. Peled, D. Golodnitsky, G. Ardel, J. Electrochem. Soc. 144 (1997) L208.
[9] M. Winter, J.O. Besenhard, M.E. Spahr, P. Novák, Adv. Mater. 10 (1998) 725.
[10] P. Novák, F. Joho, R. Imhof, J.-C. Panitz, O. Haas, J. Power Sources 81/82 (1999) 212.
[11] F. Joho, B. Rykart, R. Imhof, P. Novák, M.E. Spahr, A. Monnier, J. Power Sources 81/82 (1999) 243.
[12] P. Novák, W. Scheifele, F. Joho, O. Haas, J. Electrochem. Soc. 142 (1995) 2544.
[13] F. Joho, B. Rykart, A. Blome, P. Novák, H. Wilhelm, M.E. Spahr, J. Power Sources 97–98 (2001) 78–82.
[14] J.-C. Panitz, P. Novák, O. Haas, Appl. Spectrosc., in press.
[15] J.-C. Panitz, F. Joho, P. Novák, Appl. Spectrosc. 53 (1999) 1188.
[16] D. Alliata, R. Kötz, P. Novák, H. Siegenthaler, Electrochem. Commun. 2 (2000) 436.
[17] R. Imhof, P. Novák, J. Electrochem. Soc. 145 (1998) 1081.
[18] P. Novák, J.-C. Panitz, F. Joho, M. Lanz, R. Imhof, M. Coluccia, J. Power Sources 90 (2000) 52–58.
[19] M. Lanz, P. Novák, manuscript in preparation.
[20] B.A. Johnson, R.E. White, J. Power Sources 70 (1998) 48.
[21] F. Joho, P. Novák, O. Haas, A. Monnier, F. Fischer, Mol. Cryst. Liq. Cryst. 310 (1998) 383.
[22] M. Winter, P. Novák, A. Monnier, J. Electrochem. Soc. 145 (1998) 428.
[23] M. Inaba, H. Yoshida, Z. Ogumi, T. Abe, Y. Mizutani, M. Asano, J. Electrochem. Soc. 142 (1995) 20.
[24] D. Aurbach, B. Markovsky, A. Schechter, Y. Ein-Eli, H. Cohen, J. Electrochem. Soc. 143 (1996) 3809.

[25] M. Dollé, S. Grugeon, A. Cressent, B. Beaudoin, L. Dupont, J.-M. Tarascon, Extended abstract no. 93, in: Proceedings of the 10th International Meeting on Lithium Batteries, Como, Italy, 2000.
[26] Z. Ogumi, A. Sano, M. Inaba, T. Abe, Extended abstract no. 148, in: Proceedings of the 10th International Meeting on Lithium Batteries, Como, Italy, 2000.
[27] Z. Zhang, D. Fouchard, J.R. Rea, J. Power Sources 70 (1998) 16.
[28] L. Fransson, A.M. Andersson, A. Hussénius, K. Edström, Extended abstract no. 82, in: Proceedings of the 10th International Meeting on Lithium Batteries, Como, Italy, 2000.
[29] A. DuPasquier, F. Disma, T. Bowmer, A.S. Gozdz, G. Amatucci, J.-M. Tarascon, J. Electrochem. Soc. 145 (1998) 472.
[30] O. Haas, E. Deiss, P. Novák, W. Scheifele, A. Tsukada, Electrochem. Soc. Proc. Ser. PV 97-18 (1997) 451.
[31] T. Zheng, A. Gozdz, G.G. Amatucci, J. Electrochem. Soc. 146 (1999) 4014.